PCCP

Accepted Manuscript

ROYAL SOCIETY OF CHEMISTRY

www.rsc.org/pccp

Random lattice deformations in activated crystals are quantified by widths of the distribution function estimated from comparisons of the simulated and measured spectral envelopes

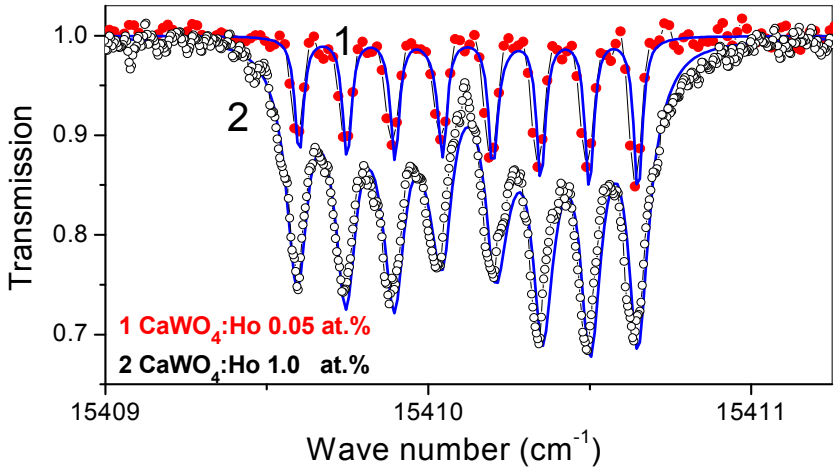

PCCP

RSCPublishing

ARTICLE

Random strain effects in optical and EPR spectra of electron-nuclear excitations in $CaWO_4$:Ho^{3+} single crystals

Cite this: DOI: 10.1039/xoxxoooooox

Received ooth January 2012,
Accepted ooth January 2012

DOI: 10.1039/xoxxoooooox

www.rsc.org/

G. S. Shakurov,[a] E. P. Chukalina,[b] M. N. Popova, [b] B. Z. Malkin[c] and A. M. Tkachuk[d]

We study paramagnetic Ho^{3+} centers in $CaWO_4$, a promising material for applications in quantum electronics and quantum information devices. Oriented single crystals with nominal holmium concentrations 0.05, 0.5, and 1 at.% were investigated at 4.2 K using EPR spectroscopy in the frequency range 37 - 850 GHz at temperatures 5-40 K and high-resolution optical transmission spectroscopy in the infrared and visible wave-length ranges. Along with the tetragonal Ho^{3+} centers of the S_4 point symmetry, four different types of low-symmetry centers were identified in the EPR spectra and their spectral parameters were determined. Well resolved hyperfine structure exhibiting holmium concentration dependent features was observed in optical spectra. Modeling of the spectra with taking into account random lattice strains gave a possibility to reproduce satisfactorily the measured hyperfine structure of the EPR signals, in particular, at anticrossings of the electron-nuclear sublevels of the ground non-Kramers doublet, and the envelopes of the hyperfine structure of optical transitions. The widths of the probability distribution of random deformations related to the point lattice defects in the samples with different concentrations of the impurity Ho^{3+} ions were estimated from a comparison of the simulated spectra with the experimental data.

Introduction

Crystals with the structure of scheelite ($CaWO_4$, space group $I4_1/a$, №88) activated by rare earth (RE) ions were extensively studied during several decades by means of optical and EPR spectroscopy. These crystals are used as active media in solid state lasers, scintillators, and frequency converters, they are also considered as promising materials for quantum computers.[1-3] For applications in optical and microwave quantum information technologies, long lifetimes and coherence times of excitations in a quantum system are crucial. This can be achieved when dealing with electron-nuclear states of RE ions. Besides importance for applications in quantum informatics, manipulation of electron-nuclear states by an external magnetic field gives a possibility to reveal and study macroscopic quantum effects induced by quantum tunneling at anticrossings of these states. Earlier, different effects at the anticrossings of hyperfine sublevels of the Ho^{3+} ion were observed in submillimeter EPR spectra and magnetization dynamics of $LiY_{1-x}Ho_xF_4$ crystals isostructural with scheelite.[4,5] In particular, anticrossings induced by low-symmetry crystal lattice distortions were found. Meanwhile, the most pronounced changes of the EPR signals were registered in the samples enriched with ^7Li or ^6Li, i.e., samples with suppressed isotopic disorder in the lithium sublattice.[4,5] By contrast with $LiYF_4$ crystals, a nonuniform isotopic composition in $CaWO_4$ crystals is of no significance, because the relative mass defects in calcium and tungsten sublattices are small as compared with the relative mass differences of ^7Li and ^6Li in $LiYF_4$. Another advantage of $CaWO_4$ over $LiYF_4$ is that in $CaWO_4$ an interaction of impurity paramagnetic ions with the nuclear spin bath is substantially suppressed. The nearest neighbors of RE ions substituting for the Ca^{2+} ions at the sites with the S_4 point symmetry are oxygen ions (see Fig. 1) with zero nuclear magnetic moments, and a single magnetic tungsten isotope ^{183}W (nuclear spin I=1/2) has a natural abundance of 14% and small nuclear gyromagnetic ratio $\gamma/2\pi$=1.75 MHz/T. Thus, a detailed study of the electron-nuclear states of impurity Ho^{3+} ions in $CaWO_4$ is, without any doubt, of great interest for applications in quantum information technologies.

Low-resolution (≈ 1 cm^{-1}) optical absorption and emission spectra of $CaWO_4$:Ho^{3+} crystals with holmium concentrations 0.5-6.0 at.% grown from a melt containing Na^+ ions (similarly to RE ions, alkali metal ions substitute for Ca^{2+} ions and compensate the excess charge of the Ho^{3+} ions) were measured earlier in Ref. 6. The spectra involved, mainly, lines related to the Ho^{3+} ions at the sites of S_4 symmetry with non local charge compensation. Crystal-field energies of the ^5I_J (J=4 - 8) multiplet sublevels and symmetries of the corresponding wave functions were determined and described by the set of crystal-field parameters defined in the coordinate system with the z axis parallel to the lattice tetragonal symmetry axis c, but

with an unknown orientation of the *x* and *y* axes relative to the crystallographic *a* and *b* axes. EPR spectra of $CaWO_4$:Ho^{3+} samples grown from the melt with the holmium and sodium concentrations 0.1 % and 1.5 %, respectively, were measured at liquid helium temperatures in the X and Q bands in Ref. 7. Spectral parameters (the *g*-factor, the hyperfine structure constant, and the most probable value of the zero-field splitting of the ground doublet) were determined. The observed distribution of the zero-field splitting of the ground non-Kramers doublet as well as the asymmetry of the lines in the low-frequency EPR spectra were interpreted as a result of the dynamical Jahn-Teller effect; however, as it is shown below, this assumption about the single-ion origin of local lattice deformations is at variance with the observed changes of the hyperfine structure of optical transitions in the concentration series of $CaWO_4$:Ho^{3+} samples. Some specific peculiarities of non resonant absorption of low-frequency acoustic and electro-magnetic fields at anticrossings of the electron-nuclear states in $CaWO_4$:Ho^{3+} single crystals were described in Ref. 8.

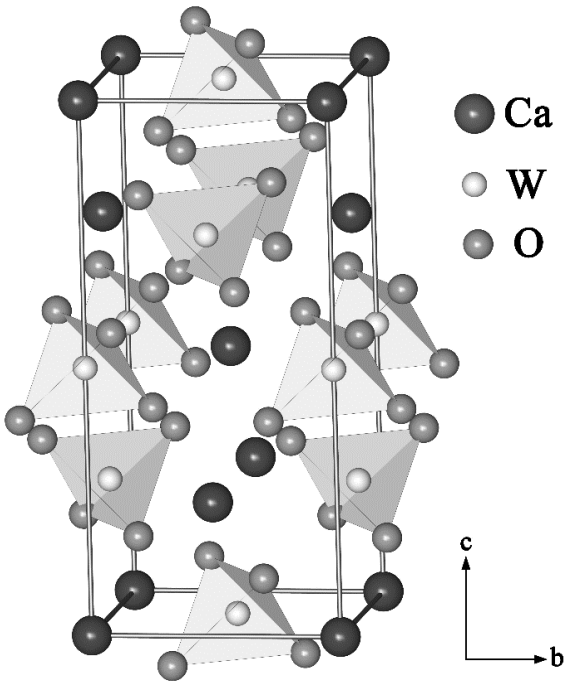

Fig. 1 Fragment of the $CaWO_4$ crystal lattice.

In the present study, spectra of electron-nuclear excitations in $CaWO_4$:Ho^{3+} crystals were measured by making use of high-resolution optical Fourier spectroscopy and tunable submillimeter EPR spectroscopy. Theoretical modeling of the EPR signal shapes and envelopes of the hyperfine structure in optical spectra of paramagnetic crystals developed earlier in Refs. 4, 9-11 is further elaborated in the present work. A comparison of the measured and simulated envelopes of the hyperfine structure of different transitions gave a possibility to determine more precisely the spectral parameters of the Ho^{3+} ions in $CaWO_4$ and to reveal specific spectral features induced by random deformations of the crystal lattice.

Experimental details

Single crystals of $CaWO_4$ doped with the Ho^{3+} ions were grown by Czochralski method using the inductive heating of the conducting crucible. The batch contained Ho_2O_3 and WO_3 oxides and $CaCO_3$, Li_2CO_3 carbonates. For spectroscopic measurements, the rectangular parallelepipeds with dimensions 6 x 3 x 2.5 mm^3 along the crystallographic axes *a*, *b*, and *c*, respectively, were cut out the oriented single crystals (the lattice constants are $a=b=0.5243$ nm, $c=1.1374$ nm.[12] Nominal holmium concentrations in the samples studied in the present work were 0.05, 0.5, and 1 at.%. One of the samples with the nominal holmium concentration 0.05 at.% was grown from the melt containing sodium carbonate instead of lithium carbonate.

The EPR spectra were measured at liquid helium temperature in steady magnetic fields $\boldsymbol{B}$ with the strength up to 1 T and alternating magnetic fields $\boldsymbol{B}_1$ parallel or normal to the field $\boldsymbol{B}$, using a tunable EPR spectrometer with backward wave oscillators generating radiation in the frequency range 37-850 GHz. A detailed description of the spectrometer was presented in Ref. 13.

Optical transmission spectra were registered using a Fourier-transform spectrometer Bruker IFS 125HR in the spectral range 5000 – 16000 cm^{-1} with a spectral resolution up to 0.01 cm^{-1}. The sample was in an optical closed-cycle Cryomech ST430 helium cryostat at temperatures 5 - 40 K stabilized within ±0.05 K. Measurements were carried out in different polarizations, with the fixed direction of the radiation wave vector $\boldsymbol{k}$ parallel or perpendicular to the sample symmetry axis *c* (α -polarization: $\boldsymbol{k} \| c$, $\boldsymbol{E}, \boldsymbol{H} \perp c$; σ -polarization: $\boldsymbol{k} \perp c$, $\boldsymbol{E} \perp c$, $\boldsymbol{H} \| c$; π -polarization: $\boldsymbol{k} \perp c$, $\boldsymbol{E} \| c$, $\boldsymbol{H} \perp c$).

Experimental results

Multiplets of the Ho^{3+} ion (with the electronic $4f^{10}$ shell) split in the crystal field of the S_4 symmetry into singlets Γ_1, Γ_2 and doublets Γ_{34} (here Γ_k are irreducible representations of the point symmetry group S_4). The lowest multiplet $^5I_8$ splits into 13 sublevels and, according to the literature data,[6] the ground state is a non-Kramers doublet Γ_{34}^1, the nearest excited states are singlets Γ_2^1 and Γ_2^2 with energies 9 and 22 cm^{-1}, respectively.

Signals with a resolved hyperfine structure corresponding to several different types of paramagnetic centers were observed in the EPR spectra of all the samples studied. There is a single holmium isotope ^{165}Ho with the nuclear spin $I=7/2$, and the EPR signals consisting of eight hyperfine components are easily identified. We consider here the results of measurements of the EPR spectra corresponding to transitions between the electron-nuclear sublevels of the ground doublet and the first and second excited singlets (see Fig. 2) only, because the EPR spectra corresponding to transitions between hyperfine sublevels of the ground doublet were described earlier in Ref. 7. It should be noted that we have not succeeded in observing transitions between the excited singlets in any of the samples, probably, because of a small population of the Γ_2^1 singlet at liquid helium temperatures. The measured resonance frequency dependences on the magnetic field $\boldsymbol{B}$ parallel to the *c* axis for the transitions between hyperfine sublevels of the ground doublet and the two nearest singlets in the tetragonal centers are presented in Fig.

3. The energies of the singlet states were determined from an analysis of these dependences. The obtained values (gaps between the centers of gravity of the hyperfine sublevels) equal 275 GHz and 665 GHz, in agreement with the optical data (see Table 1). When the field $\boldsymbol{B}$ is declined from the c axis, additional lines appear in the signals from the tetragonal centers due to mixing of electron-nuclear states with different projections of the nuclear spin moment on the c axis.

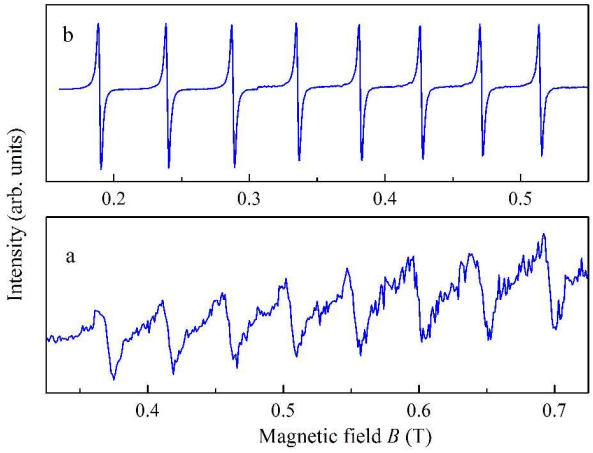

Fig. 2 EPR signals in a $CaWO_4$:Ho^{3+} (0.05 at.%) single crystal at the frequencies (*a*) 715.2 GHz and (b) 239 GHz. T=4.2 K, $\boldsymbol{B}\|c$.

Along with the most intensive signals from the tetragonal centers, the EPR spectra of all the samples studied in the present work contain lines corresponding to singlet-singlet transitions in four different centers of lower symmetry with magnetic multiplicity K_M=4 (see Fig. 4). The low-symmetry centers are marked below by symbols R1, R2, R3, and R4; measured zero-field gaps Δ between the two lowest crystal-field energy levels equal 40, 56, 126, and 190 GHz, respectively. Intensities of the EPR signals of these centers strongly depend on the polarization of the microwave radiation relative to the direction of a constant magnetic field. We suppose that low-symmetry paramagnetic centers are formed by Ho^{3+} ions close to a vacancy or a Li^+ (Na^+) compensator ion which substitutes for the Ca^{2+} ion in a neighboring position. So, for a Ho^{3+} ion at the origin of the system of coordinates, the nearest defects which perturb the crystal field can be located at the sites with the following radius-vectors [a 0 0], [a/2 a/2 c/2], [a/2 0 c/4], and [a/2 a c/4]. EPR signals from different centers in a magnetic field $\boldsymbol{B}\|c$ are shown in Fig. 4, the corresponding dependences of the resonance frequencies on the magnetic field strength for the low-symmetry centers are presented in Fig. 5. At an arbitrary deviation of the field $\boldsymbol{B}$ from the c axis, the spectral lines of low-symmetry centers split, in a general case, into four components. Because the goniometer device had only one degree of freedom, the magnetic field $\boldsymbol{B}$ could be oriented along the crystallographic c axis of a sample with an inaccuracy of ±2°. Such an error practically did not affect the resonance line position in the case of tetragonal centers with the transition frequencies linear in $\cos\theta$, where θ is the angle between the field $\boldsymbol{B}$ and the c axis. However, due to this magnetic field misorientation relative to the c axis, small splittings of the signals from magnetically nonequivalent low-symmetry centers were observed even for $\boldsymbol{B}\|c$. From estimations of the crystal fields affecting the Ho^{3+} ions in the perturbed centers mentioned above, it follows that the observed EPR signals can be related to transitions between singlets originating from the ground doublet of tetragonal centers split by a crystal-field component of the Γ_2 symmetry.

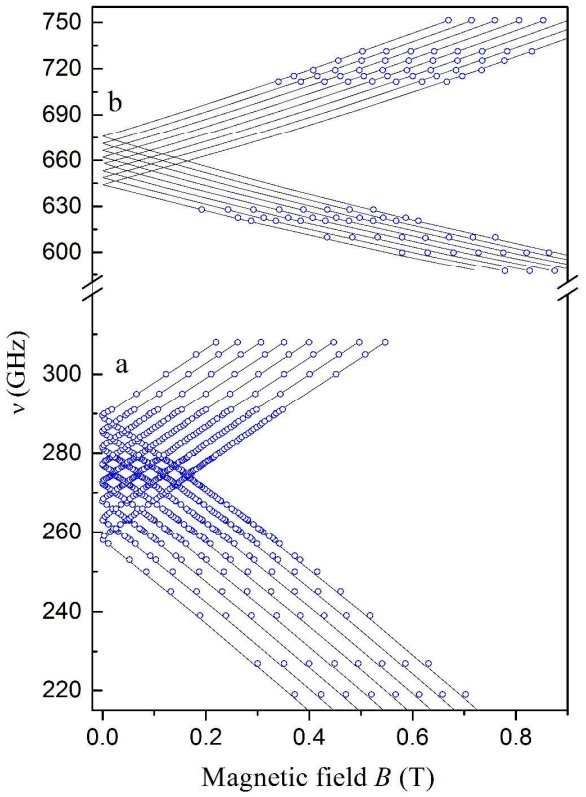

Fig. 3 Frequencies of transitions between the hyperfine components of the ground doublet and the first (*a*) and second (*b*) singlets of the Ho^{3+} ions versus magnetic field ($\boldsymbol{B}\|c$, $\boldsymbol{B}_1 \perp \boldsymbol{B}$) in a $CaWO_4$:Ho^{3+} (0.5 at.%) crystal. Symbols and solid lines correspond to the experimental data and the results of calculations, respectively.

Field dependences of the resonance frequencies ν for transitions between the hyperfine sublevels of the crystal-field singlets with a zero-field gap Δ in the EPR spectra of low-symmetry centers can be approximately described by the expression[7]

$$\nu = [\Delta^2 + (g\mu_B B + Am)^2]^{1/2} / 2\pi\hbar\,, \qquad (1)$$

where μ_B is the Bohr magneton, $\hbar$ is the Planck constant, g is the effective g-factor, A is the effective magnetic hyperfine structure constant, and $m = \pm 1/2,\ \pm 3/2,\ \pm 5/2,\ \pm 7/2$ are the nuclear spin projections on the electronic magnetic moment. As an example, the calculated dependences ν(B) in the fields $\boldsymbol{B}\|c$ for the centers R1 (Δ=40 GHz, g=12.3, A=11 GHz) and R3 (Δ=126 GHz, g=17.1, A=11.8 GHz) are presented in Fig. 5 (note that the corresponding characteristics of the ground doublet of the tetragonal centers are $g_{||}$=13.69 and A=9 GHz)[7]. From the analysis of variations of the EPR spectra induced by a rotation of the field $\boldsymbol{B}$ in the crystallographic plane ac (or bc), it follows that the effective g-factors of R1, R2, R3 and R4 centers have maximum values along the directions which are

declined from the *c* axis by angles which are not less than 37°, 30°, 17°, and 36°, respectively.

Energies of the hyperfine sublevels of the ground doublet of tetragonal centers in a magnetic field $\boldsymbol{B}\|c$ can be presented by the expression $E_m^{\pm} = \pm(g_{\|}\mu_B B + Am)/2$, where we neglect contributions from the quadrupole hyperfine interaction and random lattice deformations and take into account only terms linear in electronic Zeeman and magnetic hyperfine interactions. These sublevels cross in magnetic fields $B_{m,\Delta m} = -A(2m+\Delta m)/2g_{\|}\mu_B$ which satisfy the condition $E_m^{+} = E_{m+\Delta m}^{-}$. The most interesting effects occur at so called anticrossings when Δm is an even number, and the intersecting sublevels repel each other due to the hyperfine interaction that mixes wave functions of the doublet and the nearest singlets for $\Delta m = \pm 2$, ± 4, ± 6, or due to an interaction of the 4*f* electrons with random crystal fields of Γ_2 symmetry for $\Delta m = 0$.[4,5] Because gaps appear in the excitation spectrum of the Ho^{3+} ions at anticrossings, the shape of EPR signals in the magnetic fields with strengths equal or close to $B_{m,\Delta m} = kA/2g_{\|}\mu_B$, where *k*=1, 3, 5, 7, depends on the relation between the line width and the gap value. The widths of the EPR lines corresponding to transitions between the Γ_{34}^1 doublet and the Γ_2^1 singlet in the magnetic field $\boldsymbol{B}\|c$ measured at the frequency 208 GHz equal ~2, ~5, and ~7 mT in the samples with the holmium concentrations 0.05, 0.5, and 1 at.%, respectively.

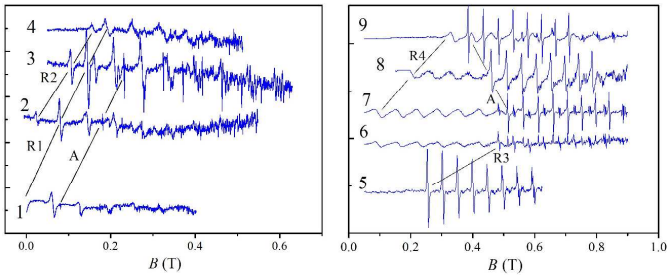

Fig. 4 EPR signals of the Ho^{3+} ions in $CaWO_4$ in the magnetic field $\boldsymbol{B}\|c$. The resonance frequencies are (1) 47.4, (2) 66.2, (3) 76, (4) 82.9, (5) 162.8, (6) 202 GHz, $\boldsymbol{B}_1\|\boldsymbol{B}$; (7) 202, (8) 208, (9) 216.5 GHz, $\boldsymbol{B}_1 \perp \boldsymbol{B}$. A- a tetragonal center, R1-R4 – low-symmetry centers. The spectra were taken for a sample with the holmium concentration 0.05 at.% except the signals 4 and 8 registered in samples with the concentrations 1 at.% and 0.5 at.%, respectively. Straight lines connect low-field components in the signals from different centers.

In the present work, detailed measurements of the EPR signals corresponding to transitions between the ground doublet Γ_{34}^1 and the first excited singlet Γ_2^1 in the tetragonal centers were carried out with a small step in the oscillator frequency variation of 0.05 GHz in the regions which involved three anticrossings with $\Delta m = 2$ and four anticrossings with $\Delta m = 0$. EPR spectra in the corresponding frequency ranges for the sample with holmium concentration 0.05 at.% are presented in Figs. 6 and 7. The EPR lines are asymmetric, this is in agreement with the measured shape of the lines corresponding to transitions between the hyperfine components of the ground doublet.[7] However, contrary to the spectra of the $^7LiYF_4:Ho^{3+}$ (0.1 %) crystal where intensities of EPR lines decrease in the regions of the anticrossings with Δm=2,[4] line intensities increase at these anticrossings in the spectra of $CaWO_4:Ho^{3+}$ (0.05 %) crystals (see Fig. 6) which gives evidence for the gap values smaller than the line width (usually, such an effect is observed in the case of overlapping lines).

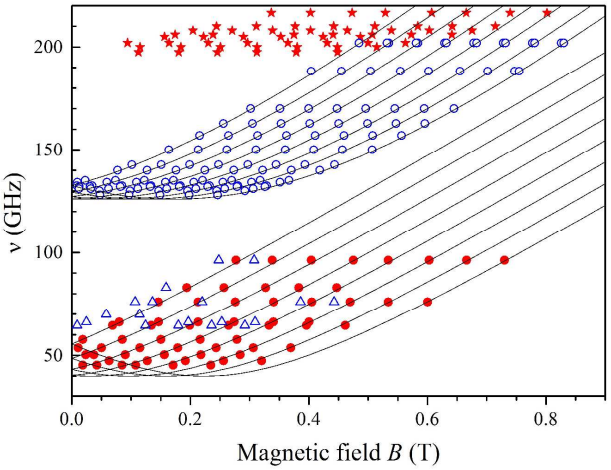

Fig. 5 Measured dependences of resonance frequencies of singlet-singlet transitions in low-symmetry centers on the magnetic field $\boldsymbol{B}\|c$. Filled circles - R1, triangles - R2, open circles - R3, stars - R4. Calculated dependences for the centers R1 and R3 are represented by solid curves.

A decrease of intensities of the EPR signals is observed at the anticrossings with Δm=0 (Fig. 7), but this effect is weaker than in the spectra of the $^7LiYF_4:Ho^{3+}$ (0.1 %) crystal.[4] When the strength of the magnetic field approaches an anticrossing point (Δm=0), intensities of both signal components decrease. In particular, the spectra registered at the frequencies 275.2 and 274.2 GHz (see Fig. 7) demonstrate increase and decrease, respectively, of the line intensities with increasing magnetic field strength.

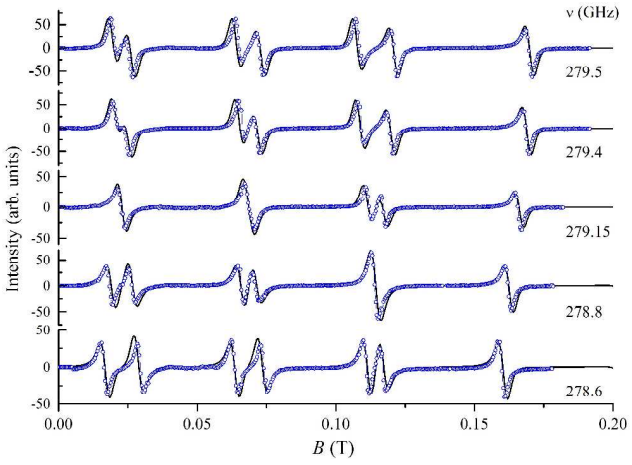

Fig. 6 Measured (symbols) and simulated (solid curves) EPR spectra in a $CaWO_4:Ho^{3+}$ (0.05 at.%) crystal in the regions of anticrossings of the electron-nuclear sublevels of the Ho^{3+} ground doublet with Δm=2 ($\boldsymbol{B}\|c$).

In the regions of the oscillator frequencies and magnetic field strengths corresponding to real crossings of the electron-nuclear sublevels (when Δm is an odd number), the evolution of the EPR spectra is the same as that observed in the vicinity of the anticrossings with Δm=2.

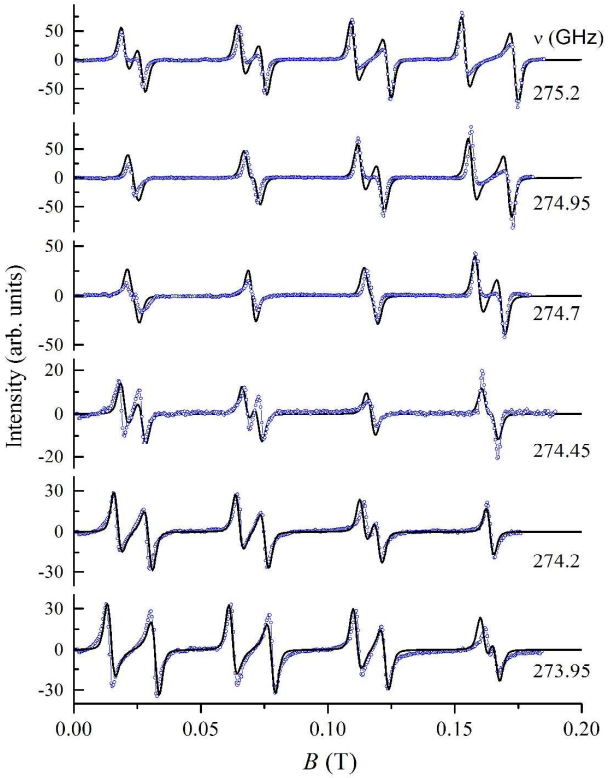

Fig. 7 Measured (symbols) and simulated (solid curves) EPR spectra in a $CaWO_4$:Ho^{3+} (0.05 at.%) crystal in the regions of anticrossings with Δm=0 (***B***||*c*).

The results of optical transmission measurements were analyzed with taking into account selection rules for electric and magnetic dipole transitions. In the crystallographic system of coordinates (*x*||*a*, *y*||*b*, *z*||*c*), the *x* and *y* components of electric (***D***) and magnetic (***M***) dipole moments of a Ho^{3+} ion in a crystal field of S_4 symmetry transform according to the Γ_{34} representation of the S_4 point group, but D_z and M_z components transform according to the Γ_2 and Γ_1 representations, respectively. If the incident radiation propagates along the symmetry axis *c* of a sample (α-polarization), optical transitions between Γ_{34} doublets and Γ_1, Γ_2 singlets can be observed only. A number of the observed lines in α-polarized spectra in each measured optical multiplet exceeds a number of allowed transitions in the tetragonal centers at low temperatures when only the ground doublet and the first excited singlet are populated. Thus, the data obtained by means of optical spectroscopy confirm the results of the EPR measurements, namely, an existence of tetragonal centers formed by the Ho^{3+} ions at the Ca^{2+} sites with a non-local compensation of the excess trivalent holmium ion charge as well as of low-symmetry centers with local charge compensation in all the samples studied. In the low-symmetry centers, degeneracy of electronic states is lifted entirely, differences between energies of the hyperfine sublevels of singlet electronic states, which are of second order in the hyperfine interaction, are small as compared to the line widths, and the hyperfine structure of these lines is not observed. However, the low-symmetry centers with relatively weak perturbation of the tetragonal crystal field and, consequently, with a small splitting of the ground Γ_{34} doublet may provide an exception.

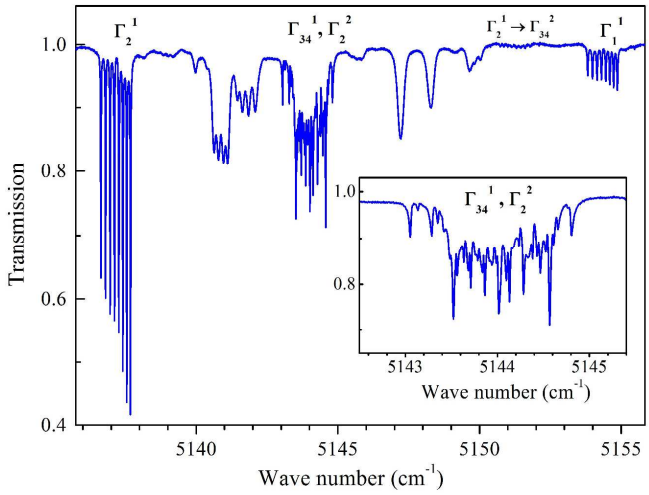

Fig. 8 Fragment of the transmittance spectrum of a $CaWO_4$:Ho^{3+} (0.05 at.%) sample in the region of the transitions between the $^5I_8$ and $^5I_7$ multiplets. *T*=5 K, α-polarization. Inset: the enlarged region of the transitions $\Gamma_{34}^1(^5I_8) \rightarrow \Gamma_{34}^1, \Gamma_2^2(^5I_7)$.

It is easy to identify spectral lines of tetragonal centers when the hyperfine structure of a line is resolved. However, this structure is observed only in the low-frequency region of optical multiplets because the homogeneous line width caused by the lifetime shortening due to nonradiative transitions increases quickly with the energy of the excited crystal-field sublevel within a given multiplet. Fragments of low-temperature transmission spectra of the $CaWO_4$:Ho^{3+} (0.05 at.%) crystal which contain lines with a well resolved hyperfine structure are presented in Figs. 8 and 9. The hyperfine structure observed in the region of the $^5I_8 \rightarrow {}^5I_7$ transitions (see Fig. 8) at low temperatures is displayed by the transitions starting from the ground doublet ($\Gamma_{34}^1(^5I_8) \rightarrow \Gamma_2^1(^5I_7)$ (Fig. 10), $\Gamma_2^2(^5I_7)$ (see inset in Fig. 8), $\Gamma_1^1(^5I_7)$ (Fig. 11*b*), $\Gamma_{34}^2(^5I_7)$ (Fig. 12*a*)) as well as from the nearest excited singlet $\Gamma_2^1(^5I_8)$ to the doublet $\Gamma_{34}^2(^5I_7)$ (Fig. 11*a*). Irregular hyperfine structure of the transition $\Gamma_{34}^1(^5I_8) \rightarrow \Gamma_2^2(^5I_7)$ is caused by a strong mixing of wave functions of the closely spaced $\Gamma_2^2(^5I_7)$ singlet and $\Gamma_{34}^1(^5I_7)$ doublet by the hyperfine interaction. Transitions between the doublets are induced by the π-polarized radiation. In this case, hyperfine structure intervals are different for the electric and magnetic dipole transitions and depend on the relative signs of the effective hyperfine structure constants of the doublets connected by a transition. The total width of the hyperfine structure can be equal either to a sum or to a difference of total hyperfine splittings of the doublets. The central intensive peak in the line $\Gamma_{34}^1(^5I_8) \rightarrow \Gamma_{34}^2(^5I_7)$ (see Fig. 12*a*) corresponds to the magnetic dipole transitions (eight hyperfine components are not resolved because of approximately equal

intervals in the hyperfine structures of the $\Gamma_{34}^1(^5I_8)$ and $\Gamma_{34}^2(^5I_7)$ doublets), and eight weak satellites correspond to the electric dipole transitions. Two close bands with four-component structures in the region of 5141-5143 cm^{-1} (see Fig. 8) can be related to transitions in the low-symmetry R1 centers with a minimal zero-field splitting of the ground quasi-doublet determined from the EPR spectra.

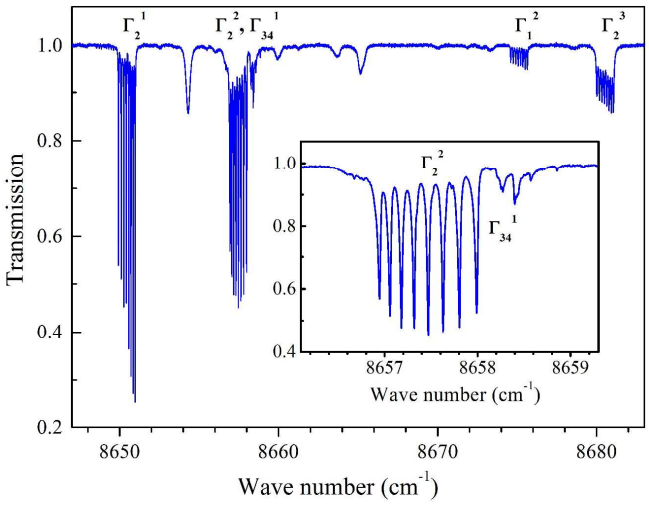

Fig. 9 Fragment of the transmittance spectrum of a $CaWO_4$:Ho^{3+} (0.05 at.%) sample in the region of the transitions between the $^5I_8$ and $^5I_6$ multiplets. T=5 K, α-polarization. Inset: the enlarged region of the transitions $\Gamma_{34}^1(^5I_8) \rightarrow \Gamma_2^2, \Gamma_{34}^1(^5I_6)$.

Well pronounced hyperfine structure of spectral lines corresponding to the $^5I_8 \rightarrow {}^5I_6$ transitions (see Fig. 9) is observed for the transitions $\Gamma_{34}^1(^5I_8) \rightarrow \Gamma_2^1(^5I_6)$ (Fig. 13*a*), $\Gamma_2^2(^5I_6)$ (Fig. 13*b*), $\Gamma_{34}^2(^5I_6)$ (Fig. 12*b*), $\Gamma_1^2(^5I_6)$ (Fig. 13*c*), and $\Gamma_2^3(^5I_6)$ (Fig. 13*d*). For the $\Gamma_{34}^1(^5I_8) \rightarrow \Gamma_2^2(^5I_6)$ line (Fig. 13*b*), a distribution of the integral intensity between the hyperfine components of the electric dipole transition is modified due to an intermixing of the $\Gamma_2^2(^5I_6)$ singlet and $\Gamma_{34}^1(^5I_6)$ doublet wave functions by the hyperfine interaction. A weak line with a resolved hyperfine structure is observed at low temperatures in the range of wave numbers close to 8649 cm^{-1}. The intensity of this line increases markedly with the temperature increasing, and we relate it to the transition from the excited $\Gamma_2^1(^5I_8)$ singlet to the $\Gamma_{34}^1(^5I_6)$ doublet. According to Ref. 6, the lowest crystal-field sublevel of the $^5I_6$ multiplet is the Γ_2 singlet, and three next sublevels, Γ_2^2, Γ_1^1, and Γ_{34}^1, lie about 8 cm^{-1} higher within the narrow range of wave numbers of an order of one cm^{-1} (see Table 1). However, we have not found any line that might be identified with transitions to the Γ_1^1 singlet in the high-resolution spectra measured in the present work.

Within the region of the $^5I_8 \rightarrow {}^5F_5$ transitions, the hyperfine structure is displayed only by the lines at 15410.1 cm^{-1} (Fig. 14) and 15437.7 cm^{-1} which correspond to transitions from the ground doublet to the lower singlets $\Gamma_2^1(^5F_5)$ and $\Gamma_1^1(^5F_5)$. The widths of the hyperfine components of these lines in the $CaWO_4$:Ho (0.05 at.%) at the temperature 5 K equal 0.033 cm^{-1} and 0.067 cm^{-1}, respectively.

Within the region of the $^5I_8 \rightarrow {}^5I_5$ transitions, the hyperfine structure of the strong transition from the ground doublet to the lowest sublevel, the $\Gamma_{34}^1(^5I_5)$ doublet, is hidden within the line width, however, well resolved structure with the widths of components 0.05 cm^{-1} is observed for the transition to this doublet from the singlet $\Gamma_2^1(^5I_8)$. A resolved hyperfine structure is seen also for the transitions from the ground doublet to the $\Gamma_2^1(^5I_5)$ and $\Gamma_1^2(^5I_5)$ singlets and the $\Gamma_{34}^2(^5I_5)$ doublet.

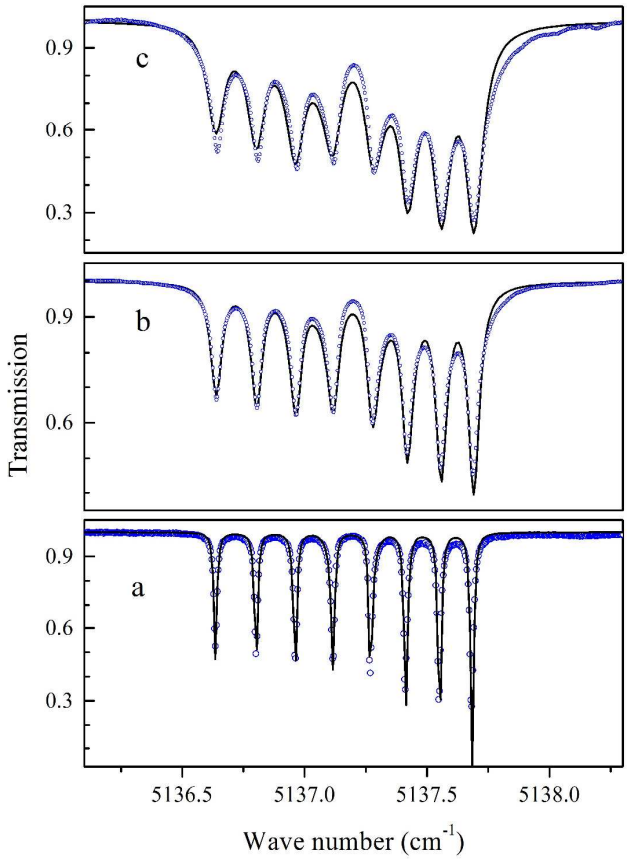

Fig. 10 Measured (symbols) and simulated (curves) hyperfine structure of the magnetic dipole transition $\Gamma_{34}^1(^5I_8) \rightarrow \Gamma_2^1(^5I_7)$ in $CaWO_4$:Ho^{3+} single crystals with nominal holmium concentrations (*a*) 0.05 at.% (parameters used in simulation: $\gamma_d = 6 \cdot 10^{-5}$, $\Delta_{\Gamma\Gamma'} = 0.008$ cm^{-1}); (*b*) 0.5 at.% ($\gamma_d = 18 \cdot 10^{-5}$, $\Delta_{\Gamma\Gamma'} = 0.026$ cm^{-1}), and (*c*) 1 at.% ($\gamma_d = 25 \cdot 10^{-5}$, $\Delta_{\Gamma\Gamma'} = 0.040$ cm^{-1}). T= 5 K. (*a*) α-polarization, (*b,c*) σ-polarization.

As follows from the EPR measurements in the region of the anticrossings with $\Delta m = 0$ in the sample with nominal holmium concentration 0.05 at.%, the most probable splitting of the ground doublet due to random lattice strains is of the order of 0.01 cm^{-1} which is much less than intervals (of about 0.15 cm^{-1}) in the hyperfine structure of this doublet. Correspondingly, no explicit signs of lattice strains are observed in the hyperfine structure patterns of optical transitions in this sample in the absence of an external magnetic field. However, in the spectra of samples with higher holmium concentrations, the eight components in the hyperfine structure of doublet-singlet transitions are separated by a

gap into two groups of four components each (examples are shown in Figs. 10 and 14). The gap increases with holmium concentration evidencing a ground doublet splitting induced by random low-symmetry components of the crystal field.

Crystal-field energies of the Ho^{3+} ions in the main centers with the S_4 point symmetry obtained from the analysis of the registered optical spectra are given in Table 1.

Table 1 Crystal-field energies (cm^{-1}) of the Ho^{3+} ions in the S_4 symmetry positions of $CaWO_4$.

Multiplet Symmetry		Measured		Calculated
		Present work	Ref. 6	
1		2	3	4
$^5I_8$	Γ_{34}^1	0	0	0
	Γ_2^1	9.16	9	9.14
	Γ_2^2	22.17	22	20.57
	Γ_1^1	-	40	46.35
	Γ_1^2	-	46	52.67
	Γ_{34}^2	-	70	70.7
	Γ_1^3	-	200	202.5
	Γ_2^3	-	248	265.8
	Γ_1^4	-	254	252.7
	Γ_{34}^3	-	262	259.9
	Γ_{34}^4	-	284	276.9
	Γ_1^5	-	300	274.8
	Γ_2^4	-	325	294.9
$^5I_7$	Γ_2^1	5137.2	5138	5137.8
	Γ_{34}^1	5143.5	5145	5143.4
	Γ_2^2	5144.0	5145	5145.1
	Γ_1^1	5154.4	5156	5153.4
	Γ_{34}^2	5160.5	5162	5166.2
	Γ_1^2	5189.0	5188	5188.4
	Γ_{34}^3	5207.5	5209	5210.5
	Γ_2^3	5218.4	5218	5218.0
	Γ_2^4	5269	5271	5271.5
	Γ_{34}^4	5274	5275	5274.5
	Γ_1^3	-	5275	5276.2
$^5I_6$	Γ_1^1	-	8661	8651.2
	Γ_2^1	8650.5	8653	8651.6
	Γ_2^2	8657.4	8661	8661.1
	Γ_{34}^1	8658.2	8662	8655.5
	Γ_{34}^2	8669.8	8674	8664.0
	Γ_1^2	8675.1	8677	8671.0
	Γ_2^3	8680.5	8683	8677.2
	Γ_1^3	8751.1	8753	8751.3
	Γ_{34}^3	8763.2	8766	8762.8
	Γ_2^4	8773.9	8776	8773.2
$^5I_5$	Γ_{34}^1	11209.8	11213	11210
	Γ_1^1	-	11215	11212
	Γ_2^1	11221.2	11215	11225
	Γ_1^2	11227.3	11229	11219
	Γ_{34}^2	11230.4	11232	11218
	Γ_1^3	-	11288	11281
	Γ_{34}^3	-	11310	11303
	Γ_2^2	-	11313	11307
$^5I_4$	Γ_1^1	-	13180	13166
	Γ_{34}^1	-	13253	13237
	Γ_2^1	-	-	13303
	Γ_1^2	-	13308	13301
	Γ_2^2	-	-	13308
	Γ_{34}^2	-	13388	13380
	Γ_1^3	-	13499	13492
$^5F_5$	Γ_2^1	15410.1	-	15420
	Γ_{34}^1	15427.5	-	15425
	Γ_1^1	15437.7	-	15443
	Γ_1^2	15478.4	-	15482
	Γ_{34}^2	15544	-	15550
	Γ_2^2	15551.8	-	15557
	Γ_1^3	15568	-	15566
	Γ_{34}^3	15585	-	15591

This scheme of energy levels, the measured hyperfine structure patterns and field dependences of the resonance frequencies in the EPR spectra form a basis for developing a model to describe the electronic structure of the tetragonal holmium centers and for finding the model parameters. The next Section is devoted to this point.

Simulations of the EPR and optical spectra

The first step in modeling a spectrum of electron-nuclear excitations of a RE ion involves construction of the Hamiltonian H of the unfilled electronic $4f^N$-shell in the crystal field and numerical diagonalization of this Hamiltonian operating in the total space of C_{14}^N electronic states. Next, the operators of the hyperfine interaction and of the electronic magnetic (***M***) and effective electric (***D***) dipole moments are projected on the subspace of the lower eigenstates of H in the range of energies comparable with the energy of photons in the incident probing radiation. The matrix of the hyperfine interaction in the space of $(2I+1)d$ electron-nuclear states (I is the nuclear spin, $d \le C_{14}^N$ is the number of electronic states) is numerically diagonalized, and the obtained entangled electron-nuclear wave functions are used to calculate squares of the absolute values of matrix elements of the operators ***M*** and ***D*** which determine relative integral intensities of the corresponding spectral lines. The spectral envelopes are simulated as the sums of contributions from

all possible transitions between the hyperfine sublevels of the initial and final crystal-field levels with a varied width of the intensity distribution to match the results of measurements. When considering the EPR spectra, the Hamiltonian H is supplemented by the electronic Zeeman energy $H_Z = -\boldsymbol{MB}$, where $\boldsymbol{M} = -\mu_B(\xi\boldsymbol{L} + 2\boldsymbol{S})$, $\boldsymbol{L} = \sum_i \boldsymbol{l}_i$, and $\boldsymbol{S} = \sum_i \boldsymbol{s}_i$ are the total orbital and spin moments, respectively, of 4*f* electrons labeled by the index *i*, and ξ is the orbital reduction factor.

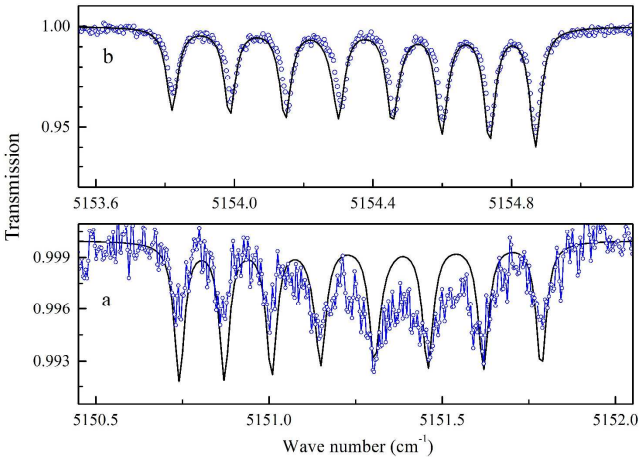

Fig. 11 Measured (symbols) and simulated (curves) envelopes of the hyperfine structure of the ${}^5I_8 \rightarrow {}^5I_7$ transitions in a $CaWO_4$:Ho^{3+} (0.05 at.%) sample: (*a*) - $\Gamma_2^1({}^5I_8) \rightarrow \Gamma_{34}^2({}^5I_7)$, $\Delta_{\Gamma\Gamma'} = 0.035$ cm^{-1}, (*b*) - $\Gamma_{34}^1({}^5I_8) \rightarrow \Gamma_1^1({}^5I_7)$, $\Delta_{\Gamma\Gamma'} = 0.038$ cm^{-1}. *T*=5 K, α-polarization.

We obtained the crystal-field energies E_Γ and the corresponding electronic wave functions ψ_Γ of the Ho^{3+} ions by numerical diagonalization of the Hamiltonian

$$H = H_{FI} + H_{CF} \qquad (2)$$

where H_{FI} is the standard free-ion Hamiltonian operating in the space of 1001 electronic states of the $4f^{10}$ configuration,[14] which involves the electrostatic interaction between the electrons, the spin-orbit interaction, corrections to the electrostatic interaction due to the configuration mixing, and relativistic terms:

$$H_{\mathrm{FI}} = \sum_i \zeta \boldsymbol{l}_i \boldsymbol{s}_i + \alpha \boldsymbol{L}^2 + \beta \hat{G}(G_2) + \gamma \hat{G}(R_7) + \sum_k (F^k \hat{f}_k + P^k \hat{p}_k + T^k \hat{t}_k + M^k \hat{m}_k). \qquad (3)$$

The calculations were carried out with making use of the parameters ζ=2133.2, α=18.9, β=-611, γ=2013, F^2=93668, F^4=66113, F^6=49372, P^2=528, P^4=396, P^6=264, T^2=249, T^3=37, T^4=98, T^6= -316, T^7=440, T^8=372, M^0=3, M^2=1.7, and M^4=1.1 (cm^{-1}) presented earlier in Ref. 15 for the impurity Ho^{3+} ions in YPO_4.

The crystal-field Hamiltonian of the 4*f* electrons localized at the sites of the Ca^{2+} ions in the perfect $CaWO_4$ lattice can be written in the crystallographic system of coordinates as follows:

$$H_{CF} = B_2^0 O_2^0 + B_4^0 O + B_4^4 O_4^4 + B_4^{-4} O_4^{-4} + B_6^0 O_6^0 + B_6^4 O_6^4 + B_6^{-4} O_6^{-4}. \quad (4)$$

Here $O_p^k = \sum_i O_p^k(i)$ $(k \le p)$ are the linear combinations of spherical tensor operators defined in Ref. 16 which coincide with the Stevens operators[17] in the space of eigenfunctions of the angular momentum. Initial values of the crystal-field parameters B_p^k were calculated in the framework of the exchange charge model[18] and then varied to fit the measured field dependences of the resonance frequencies of transitions between the hyperfine sublevels of the ground doublet and the first excited singlet (see Fig. 3*a*), the final values are presented in column B of Table 2.

Table 2 Crystal-field parameters B_p^k (cm^{-1}) of impurity RE^{3+} ions in the S_4 symmetry positions of $CaWO_4$.

p *k*	Yb^{3+} $(4f^{13})$[19]	Er^{3+} $(4f^{11})$[20]	Ho^{3+} $(4f^{10})$[6]	Dy^{3+} $(4f^{9})$[21]	Ho^{3+}, present work	
					A	B
2 0	242	231	218	214	220	220
4 0	-77	-90	-83	-103	-80.5	-80.5
4 4	773	852	815	1016	831	-593
4 -4	0	0	0	0	0	-582
6 0	-1	-0.6	-2.1	-2.1	-2.34	-2.34
6 4	355	396	391.5	314.3	430	-304
6 -4	0	-75	-137	-1.8	4	-304

The values of parameters given in column A of Table 2 were obtained from the parameters in column B as a result of a rotation of the system of coordinates around the *z*||*c* axis by the angle $11.12^o \pm 45^o$, these values are in conformity with the crystal-field parameters presented earlier for $CaWO_4$:Ho^{3+},[6] $CaWO_4$:Yb^{3+},[19] $CaWO_4$:Er^{3+},[20] and $CaWO_4$:Dy^{3+} crystals.[21] The calculated crystal-field energies E_Γ (column 4 in Table 1) within the multiplets considered in the present work are compared with the experimental data (columns 2 and 3 in Table 1). It should be noted that differences between the measured and calculated energies in Table 1 are partly caused by neglect of shifts of the energy levels induced by the electron-phonon and hyperfine interactions which are not accounted for in Eq. (2).

More than half a century ago, it was shown that specific features of EPR spectra of non-Kramers RE ions with a doubly degenerate ground state are determined by an interaction of 4*f* electrons with random deformations of the crystal lattice.[22,23] Majority of earlier published papers, beginning from Refs. 22, 23, assumed the Gaussian distribution of random lattice deformations. However, we can consider a more physically grounded form of the strain distribution and connect its width with specific characteristics of a system under study. In particular, we suppose here that random deformations are induced by point defects in the crystal lattice. A corresponding generalized distribution function of random strains in the elastic continuum was recently derived in Ref. 11. In the case of $CaWO_4$, a distribution density for random deformations of the Γ_2 symmetry which split the non-Kramers Γ_{34} doublets, $e_1(\Gamma_2) = (e_{xx} - e_{yy})/2$ and $e_2(\Gamma_2) = e_{xy}$ (here $e_{\alpha\beta}$ are the components of the deformation tensor in the crystallographic system of coordinates), takes the form

$$g(e_1, e_2) = \frac{\gamma_d}{2\pi}(e_1^2 + e_2^2 + \gamma_d^2)^{-3/2}. \qquad (5)$$

The distribution width γ_d is linear in the defect concentration.[9,11] The crystal field affecting the Ho^{3+} ions is modulated by random strains, and the corresponding Hamiltonian of the electron-deformation interaction linear in the deformation tensor components can be written as follows:

$$H_{def}=V_1e_1+V_2e_2, \quad (6)$$

where electronic operators

$$V_\lambda = \sum_{pk} b^k_{\lambda,p} O^k_p \quad (\lambda = 1, 2) \quad (7)$$

are determined by sixteen parameters $b^{\pm2}_{\lambda,p}$ (p=2, 4, 6), $b^{\pm6}_{\lambda,6}$. In the present work, we use values of the parameters $b^k_{\lambda,p}$ determined from piezospectroscopic studies of a $LiYF_4:Ho^{3+}$ crystal.[5] Below, we consider random strains of the Γ_2 symmetry in the polar coordinate system where $e_1 = \rho\cos\varphi$ and $e_2 = \rho\sin\varphi$.

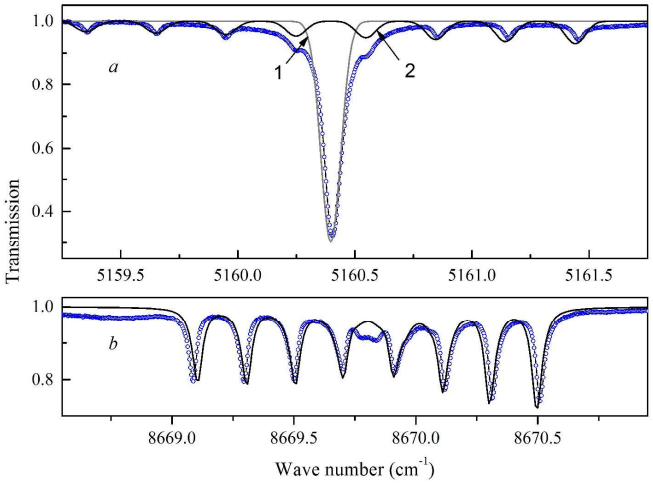

Fig. 12 Measured (symbols) and simulated (curves) hyperfine structure of the doublet-doublet transitions in a $CaWO_4:Ho^{3+}$ (0.05 at.%) sample: (*a*) - $\Gamma^1_{34}(^5I_8) \rightarrow \Gamma^2_{34}(^5I_7)$, 1- magnetic dipole transitions, 2 - electric dipole transitions, $\Delta_{\Gamma\Gamma'}$ = 0.1 cm^{-1}, (*b*) - $\Gamma^1_{34}(^5I_8) \rightarrow \Gamma^2_{34}(^5I_6)$, $\Delta_{\Gamma\Gamma'}$ = 0.023 cm^{-1}. *T*=5 K. Unpolarized light propagating along the *a* – axis of the crystal.

Thus, to analyze the electron-nuclear excitations genetically connected with the ^5I_J (J=4, 5, 6, 7, 8) and $^5F_5$ multiplets, we consider the Hamiltonian

$$H_{el-n} = H_0 + H_Z + H_{HFM} + H_{HFQ} + H_{def} \quad (8)$$

which operates in the Kronecker product of the nuclear subspace (eight functions $|I=7/2, I_z>$) and the electronic subspace of the wave functions ψ_Γ corresponding to 76 lower eigenvalues of the Hamiltonian (2). The electronic Hamiltonian H_0 is presented by a diagonal matrix $H_{0,\Gamma\Gamma'} = (E_\Gamma + e_\Gamma)\delta_{\Gamma\Gamma'}$ where the varied parameters e_Γ ($|e_\Gamma|$<10 $см^{-1}$) are added to the crystal-field energies to achieve compatibility of the simulated and measured spectral envelopes. Operators H_{HFM} and H_{HFQ} correspond to magnetic dipole and electric quadrupole hyperfine interactions, respectively:

$$H_{HFM} = V_M\{2\boldsymbol{IL} + (3O^0_{S2,z}I_z - \boldsymbol{O}^0_{S2}\boldsymbol{I}) + 3(O^2_{S2,x}I_x - O^2_{S2,y}I_y) + 3(O^{-2}_{S2,x}I_x + O^{-2}_{S2,y}I_y) + 6(O^1_{S2,x}I_z + O^1_{S2,z}I_x) + 6(O^{-1}_{S2,z}I_y + O^{-1}_{S2,y}I_z)\}, \quad (9)$$

$$H_{HFQ} = VI_0 + V_{el}[O^0_2I_0 + 3O^2_2I_2 + 3O^{-2}_2I_{-2} + 6O^1_2I_1 + 6O^{-1}_2I_{-1}]. \quad (10)$$

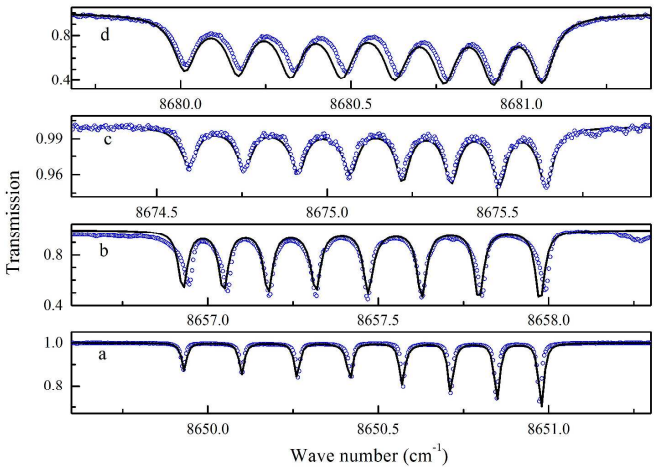

Fig. 13 Measured (symbols) and simulated (curves) hyperfine structure of the doublet-singlet transitions in a $CaWO_4:Ho^{3+}$ (0.05 at.%) sample: (*a*) - $\Gamma^1_{34}(^5I_8) \rightarrow \Gamma^1_2(^5I_6)$, $\Delta_{\Gamma\Gamma'}$=0.009 cm^{-1}, (*b*) - $\Gamma^1_{34}(^5I_8) \rightarrow \Gamma^2_2(^5I_6)$, $\Delta_{\Gamma\Gamma'}$= 0.016 cm^{-1}, (*c*) - $\Gamma^1_{34}(^5I_8) \rightarrow \Gamma^2_1(^5I_6)$, $\Delta_{\Gamma\Gamma'}$ = 0.025 cm^{-1}, (*d*) - $\Gamma^1_{34}(^5I_8) \rightarrow \Gamma^3_2(^5I_6)$, $\Delta_{\Gamma\Gamma'}$ = 0.04 cm^{-1}. *T*=5 K, α-polarization.

Here $\boldsymbol{O}^k_{S2} = \sum_i O^k_2(i)\boldsymbol{s}_i$,

$$V_M = \mu_B\gamma_N\hbar\left\langle\frac{1}{r^3}\right\rangle_{4f}, \quad V = \frac{e^2Q(1-\gamma_\infty)}{4I(2I-1)}\sum_L q_L\frac{3z_L^2 - r_L^2}{r_L^5}, \quad (11)$$

$$V_{el} = -\frac{e^2Q(1-R_Q)}{4I(2I-1)}\left\langle\frac{1}{r^3}\right\rangle_{4f}, \quad (12)$$

e is the elementary charge, $\gamma_N/2\pi$ =8.98 MHz/T is the nuclear gyromagnetic ratio, $Q = 2.394\cdot10^{-28}$ m^2 is the nuclear quadrupole moment,[24] γ_∞=-80 and R_Q=0.1 are Sternheimer antishilding and shielding factors,[25] respectively, $\boldsymbol{r}$ is the radius-vector of the 4*f* electron, the average value of $1/r^3$, $\langle 1/r^3\rangle_{4f}$, is 9.7 at. units[26], $I_0 = 3I_z^2 - I(I+1)$, $I_2 = I_x^2 - I_y^2$, $I_{-2} = I_xI_y + I_yI_x$, $I_1 = I_xI_z + I_zI_x$, $I_{-1} = I_zI_y + I_yI_z$. The first term at the right hand side of Eq. (10) corresponds to the crystal lattice contribution into the electric field gradient at the holmium nucleus, the sum in the expression for the parameter V is taken over lattice ions with charges eq_L and radius-vectors $\boldsymbol{r}_L$ relative to the holmium nucleus. The calculated according to the definitions (11,12) parameters of the hyperfine interaction are V_M=0.01804, V_{el}=-0.001934 and V=-0.000441 (cm^{-1}).

The shape of the EPR signals corresponding to resonance transitions between the hyperfine sublevels of the ground doublet $\Gamma^1_{34}(^5I_8)$ and the first singlet $\Gamma^1_2(^5I_8)$ in a magnetic field $\boldsymbol{B}\|c$ and alternating field of frequency ν normal to $\boldsymbol{B}$ is simulated as a derivative of the absorption spectrum envelope relative to the

magnetic field strength B. This envelope is defined by the expression (see Ref. 4):

$$I(B)=\int dB'\left\langle \sum_{jk}\sum_{\alpha=x,y}|<\Gamma_2^1 k|M_\alpha|\Gamma_{34}^1 j>|^2(N_j-N_k) \times\frac{\exp[-(2\pi\hbar\nu-E_{kj}(B'))^2/2\delta^2]}{(B-B')^2+\Delta B^2}\right\rangle_e . \quad (13)$$

Here intrinsic distributions of the resonance frequency and magnetic field are accounted for, $E_{kj}=E_k-E_j$, indices j=1 - 16 and k=1 - 8 enumerate the hyperfine sublevels of the doublet and the singlet with energies E_j and E_k and populations N_j and N_k, respectively. The symbol $\langle ... \rangle_e$ means averaging over the distribution of the random deformations (5), namely,

$$\langle A\rangle_e=\frac{\gamma_d}{2\pi}\int_0^\infty\frac{\rho d\rho}{(\rho^2+\gamma_d^2)^{3/2}}\int_0^{2\pi}A(\rho,\varphi)d\varphi \quad (14)$$

where $A(\rho,\varphi)$ is calculated with making use of the numerical diagonalization of the Hamiltonian (8) for fixed values of the variables ρ and φ and of the magnetic field strength B that has been varied with a step of 0.5 mT. Values of the parameters δ and ΔB which determine widths of the hyperfine structure components, and the width γ_d of the distribution function of the random strains are obtained from a comparison of the simulated and measured spectra.

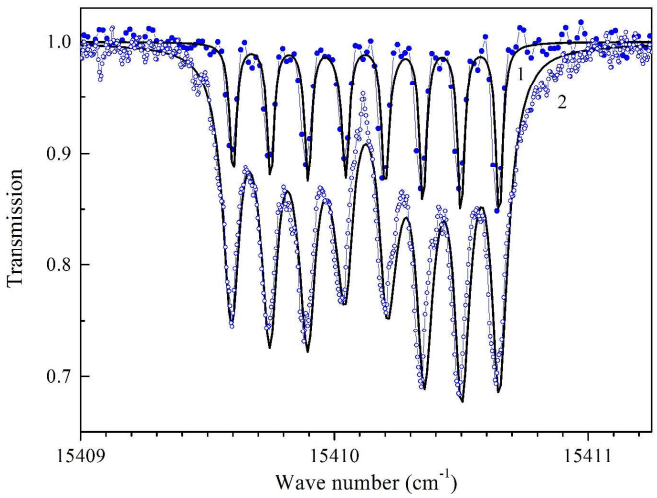

Fig. 14 Measured (symbols) and simulated (curves) hyperfine structure of the transition $\Gamma_{34}^1(^5I_8)\rightarrow\Gamma_2^1(^5F_5)$ in $CaWO_4$:Ho^{3+} single crystals with nominal holmium concentrations 0.05 at.% (1, $\gamma_d=6\cdot10^{-5}$, $\Delta_{\Gamma\Gamma'}=0.015$ cm^{-1}) and 1 at.% (2, $\gamma_d=25\cdot10^{-5}$, $\Delta_{\Gamma\Gamma'}=0.036$ cm^{-1}), T= 5 K, α-polarization.

The envelope of the hyperfine structure of the electronic transition $\Gamma\rightarrow\Gamma'$ induced by a polarized radiation ($\lambda=\alpha,\sigma,\pi$) is simulated as a function of the photon energy E (measured in wave numbers) with a step of 0.01 cm^{-1}:

$$I_{\Gamma\Gamma',\lambda}(E)=\left\langle\sum_{j\in\Gamma}\sum_{k\in\Gamma'}I_{jk}^{(\lambda)}N_j f_{\Gamma\Gamma'}(E-E_k+E_j)\right\rangle_e , \quad (15)$$

where E_j and E_k are energies of the hyperfine sublevels of the electronic states Γ and Γ', respectively (eigenvalues of the Hamiltonian (8) for zero magnetic field). The contribution into the envelope from each possible transition between the hyperfine sublevels is presented by a Lorentzian line $f_{\Gamma\Gamma'}(x)=\Delta_{\Gamma\Gamma'}/[2\pi(x^2+\Delta_{\Gamma\Gamma'}^2/4)]$ with a total width at half maximum $\Delta_{\Gamma\Gamma'}$ and a weight $I_{jk}^{(\lambda)}$ determined by the corresponding matrix elements of the magnetic or electric dipole moment components:

$$I_{m,jk}^{(\alpha,\pi)}=|<\Gamma' k|M_x|\Gamma j>|^2+|<\Gamma' k|M_y|\Gamma j>|^2,$$
$$I_{m,jk}^{(\sigma)}=|<\Gamma' k|M_z|\Gamma j>|^2, \quad (16)$$

$$I_{e,jk}^{(\alpha,\sigma)}=|<\Gamma' k|D_x|\Gamma j>|^2+|<\Gamma' k|D_y|\Gamma j>|^2,$$
$$I_{e,jk}^{(\pi)}=|<\Gamma' k|D_z|\Gamma j>|^2 . \quad (17)$$

The magnetic moment operator $\boldsymbol{M}$ has been already defined above. Operators corresponding to components of the effective electric dipole moment $D_\alpha=\sum_{p=2,4,6;\,k=\pm1,...\pm p}d_{\alpha,p}^k O_p^k$ of a RE ion in the crystal field of the S_4 symmetry are determined by nonzero parameters $d_{x,p}^{\pm1}$, $d_{y,p}^{\pm1}=\pm d_{x,p}^{\mp1}$, $d_{z,p}^{\pm2}$ (p=2,4,6), $d_{x,p}^{\pm3}$, $d_{y,p}^{\pm3}=\mp d_{x,p}^{\mp3}$ (p=4,6), $d_{x,6}^{\pm5}$, $d_{y,6}^{\pm5}=\pm d_{x,6}^{\mp5}$, $d_{z,6}^{\pm6}$. In the present work we used values of these parameters calculated in Ref. 27 for the impurity Er^{3+} ions in the isostructural $LiYF_4$ crystal. Description of the intensity distribution within an individual transition by the Lorentzian form-function includes both homogeneous and inhomogeneous broadening due to finite lifetimes of the excited states and interactions of the Ho^{3+} ions with random totally symmetric strains, respectively. It is worth noting that the observed intense pedestal that arises under the resolved hyperfine structure with increasing temperature and concentration of the impurity ions evidences wide wings in the measured spectral lines which are specific of just the Lorentzian form-function.

Discussion

A successive analysis of the EPR signals in a $CaWO_4$:Ho^{3+} (0.05 at.%) sample at the anticrossings with Δm =2 and Δm =0 gave a possibility to find values of the parameters δ and ΔB which determine widths of the electron-nuclear transitions (see Eq. (12)) and the width γ_d of the strain distribution function. However, it should be noted that, to fit the measured resonance frequencies vs field dependences of the EPR signals presented in Fig. 3, using the crystal field parameters from column B in Table 2, it was necessary to introduce the orbital reduction factor ξ=0.982, slightly different from unity. The corresponding calculated g-factor of the ground doublet $g_{\|}$=13.6924 practically coincides with the one measured in Ref. 7.

The calculated gap of 0.232 GHz between hyperfine sublevels of the ground doublet with the nuclear spin projections m=-3/2 and m'=1/2 in the magnetic field $B_{-3/2,2}$ is about 1.5 times smaller than the corresponding gap in $LiYF_4$:Ho^{3+} which is a consequence of different energies of the first excited singlet $\Gamma_2^1(^5I_8)$ of the Ho^{3+} ions in $CaWO_4$ (9.1 cm^{-1}) and $LiYF_4$ (6.8 cm^{-1}). This gap is smaller than

the line width $\Delta\nu$ =0.39 GHz of individual transitions between hyperfine sublevels of the ground doublet and the $\Gamma_2^1(^5I_8)$ singlet, correspondingly, the intensity of the EPR signals increases at the anticrossings with Δm =2. Envelopes of the EPR signals simulated using the parameters δ =0.075 GHz, ΔB =0.85 mT, and γ_d =0 reproduce very well the measured signals in the regions of the anticrossings with Δm =2 (see Fig. 6). Here, the value of δ comes from the setup form-function and is the same as in Ref. 4, the width ΔB of the magnetic field distribution is slightly smaller than in $LiYF_4$ where local magnetic fields involve contributions from the fluorine nuclear magnetic moments.[4] The calculated envelopes practically do not change when the strain distribution width γ_d does not exceed 10^{-4}. Some differences in the behavior of the EPR signal intensities in the regions of the anticrossings with Δm =2 at the fields $B_{-3/2,2}$ and $B_{-5/2,2}$, $B_{-7/2,2}$ (see Fig. 6) are caused by an unresolved structure of signals corresponding to transitions of different intensity between the ground doublet sublevel and eight hyperfine sublevels of the $\Gamma_2^1(^5I_8)$ singlet with small but finite total hyperfine splitting of 0.04 cm^{-1} (see Fig. 7 in Ref. 4).

Next, after the parameters δ and ΔB had been fixed, we found the width of the strain distribution function $\gamma_d = 6\cdot 10^{-5}$ in a $CaWO_4$:Ho^{3+} (0.05 at.%) sample from fitting the measured EPR signals at the anticrossings with Δm=0 (see. Fig. 7) by simulated envelopes (12). As one might expect, in the case of heterovalent doping random strains are stronger than in the case of homovalent substitution, even in the samples with lower concentration of impurity ions (in particular, $\gamma_d = 4.2\cdot 10^{-5}$ in the isostructural $^7LiYF_4$:Ho^{3+} (0.1 at.%) crystal).[9]

In accordance with the distribution (5), the most probable absolute value of a deformation of the Γ_2 symmetry is $\rho_M = \gamma_d/\sqrt{2}$. We define the most probable splitting of hyperfine sublevels of the ground doublet at the anticrossings with Δm =0 as an angular average of the doubled absolute value of the corresponding matrix element of the electron-deformation interaction

$$\Delta E_M(\Gamma_{34}) = \frac{\rho_M}{\pi}\int_0^{2\pi} |<+|V_1\cos\varphi + V_2\sin\varphi|->| \, d\varphi \,, \qquad (18)$$

where $|\pm>$ are the electronic wave functions of the doublet sublevels in a magnetic field $\boldsymbol{B}\parallel c$. Using the parameters of the electron-deformation interaction from Ref. 5, from Eq. (17) we obtain $\Delta E_M(\Gamma_{34}) = 186\,\gamma_d$ cm^{-1}. In a $CaWO_4$:Ho^{3+} (0.05 at.%) sample with the width of the strain distribution function presented above, the corresponding gap of 0.36 GHz in magnetic fields $B_{m,\Delta m=0}$ is comparable to the line width and is markedly smaller than the splitting 0.9 GHz of the ground doublet used in Ref. 7 for a description of the EPR spectra in a $CaWO_4$:Ho^{3+} (0.1 %) sample. Nevertheless, as is seen in Fig. 7, intensities of the EPR signals in the $CaWO_4$:Ho^{3+} (0.05 at.%) sample diminish substantially at the anticrossings with Δm =0.

It should be noted that the shapes of the EPR signals and the magnetization dynamics at anticrossings in the isostructural $LiYF_4$:Ho^{3+} crystals have been analyzed earlier in Refs. 4, 5 assuming a fixed value of the ground doublet splitting. However, in the framework of this simplified approach, some peculiarities of dynamic processes and spectral line shapes caused by a specific form of the strain distribution function (in particular, strong asymmetry of the EPR line shape) remained unrevealed.

The envelopes of spectral lines in transmission spectra of the CaWO4:Ho^{3+} (0.05 at.%) crystal at the temperature 5 K simulated in accordance with Eq. (14) are compared with the measured spectra in Figs. 10-12. The widths of individual transitions $\Delta_{\Gamma\Gamma'}$ presented in figure captions were determined from a comparison of simulated and measured hyperfine structures of the spectral lines. The analysis of observed profiles of the doublet-doublet transitions has shown that the electric dipole transitions dominate in all optical multiplets except the $^5I_7$ one. In the latter case, the magnetic dipole transitions play the main role. The calculated total hyperfine splittings Δ_{HF} of the Γ_{34} doublets (differences of the maximal and minimal energies of the corresponding electron-nuclear sublevels) are presented in Table 3. As it is seen in Figs. 11 and 13, the total width of the observed hyperfine structure of transitions from the ground doublet to excited singlets practically does not depend on the upper state. This is because a total extension of a four-component hyperfine structure of the most of the crystal-field singlets does not exceed 0.03 cm^{-1} and is at least five times smaller than intervals in the hyperfine structure of the ground doublet Γ_{34}^1 ($^5I_8$). The modeling of the hyperfine structure of the closely spaced spectral lines corresponding to transitions into Γ_{34}^1 ($^5I_7$) and Γ_2^2 ($^5I_7$), Γ_2^2 ($^5I_6$) and Γ_{34}^1 ($^5I_6$) crystal field levels gave a possibility to determine the gaps between these levels, $E(\Gamma_2^2, {}^5I_7) - E(\Gamma_{34}^1, {}^5I_7)$ = 0.23 cm^{-1}, $E(\Gamma_{34}^1, {}^5I_6)$ - $E(\Gamma_2^2, {}^5I_6)$ = 0.81 cm^{-1}, with a precision of about 0.01 cm^{-1}.

Table 3 Hyperfine splittings of non-Kramers doublets Δ_{HF} (cm^{-1}) of the Ho^{3+} ions in the S_4 symmetry positions of $CaWO_4$.

Doublet	Δ_{HF}	Doublet	Δ_{HF}	Doublet	Δ_{HF}
$^5I_8$ Γ_{34}^1	1.047	$^5I_7$ Γ_{34}^1	0.644	$^5I_6$ Γ_{34}^1	1.062
Γ_{34}^2	0.757	Γ_{34}^2	1.043	Γ_{34}^2	0.338
Γ_{34}^3	0.300	Γ_{34}^3	0.542	Γ_{34}^3	0.076
Γ_{34}^4	0.776	Γ_{34}^4	0.216		
$^5I_5$ Γ_{34}^1	1.283	$^5I_4$ Γ_{34}^1	0.829	$^5F_5$ Γ_{34}^1	0.262
Γ_{34}^2	0.545	Γ_{34}^2	0.186	Γ_{34}^2	0.068
Γ_{34}^3	0.060			Γ_{34}^3	0.679

Assuming that the width of the strain distribution contains a contribution $\Delta\gamma_d = \alpha C$ linear in the concentration C of the impurity Ho^{3+} ions, we obtain the coefficient α =0.02 from the values of the widths $\gamma_d = \gamma_0 + \alpha C$ = 6, 18, and 25 (in units of 10^{-5}, see Figs. 10, 14) determined from a modeling of the spectral envelopes in the samples with concentrations C=0.05, 0.5, and 1 at.%, respectively. Thus, we can conclude that the width $\gamma_0 = 5\cdot 10^{-5}$ corresponding to strains induced by intrinsic lattice defects dominates in the case of the $CaWO_4$ sample with the lowest nominal concentration of the impurity ions.

Conclusions

The goal of our study was to elaborate further the modeling of EPR signal shapes and envelopes of the hyperfine structure in optical spectra of impurity RE ions in crystals of different symmetry, which is of primary importance for extracting correct and precise information on the electron-nuclear states relevant for a quantum information device. The results of the present work as well as of the previously published study[9] on high-resolution optical and submillimeter EPR spectra of KY_3F_{10}:Ho^{3+} crystals demonstrate a precise description of electron-nuclear excitations in the Ho^{3+} ions at the scales of their energy variations differing up to three orders of magnitude. It is important to emphasize that a single set of parameters in the effective Hamiltonian operating in a total space of states of the unfilled electronic 4*f* shell is used. In particular, phenomenological polarization contributions are not introduced into the Hamiltonian of the magnetic hyperfine interaction.

Different profiles of the hyperfine structure of spectral lines caused by specific peculiarities of the multiplet splittings in the crystal field and by low-symmetry deformations of the crystal lattice were observed earlier[28,29] in the high-resolution optical spectra of $YAl_3(BO_3)_4$ and YPO_4 crystals containing impurity Ho^{3+} ions at the sites of the yttrium sublattices with the trigonal and tetragonal point symmetry, respectively. Basically, the methods of calculations of the spectral line frequencies employed in Refs. 28, 29 and in the present work are similar. However, the approach developed in the present work to analyze the experimental data involves calculations not only of the transition energies but also of relative transition intensities within the spectral line profile. The detailed analysis of spectral effects caused by random crystal lattice deformations based on the averaging of the observables over physically grounded strain distribution function allowed us to obtain plausible estimations of the most probable strains in the samples with different concentrations of the impurity ions. Modeling of the hyperfine structure envelopes opens a possibility to determine crystal-field energies of RE ions with a precision comparable with the spectrometer resolution, i.e., 0.01 cm^{-1}.

In conclusion, we would like to emphasize that a continuous distribution of splittings of the degenerate crystal field levels of non-Kramers RE ions at sites with cubic, tetragonal or trigonal point symmetry and of the quadruplet Γ_8 levels of Kramers RE ions at sites with cubic symmetry is a general property of real crystals containing RE ions, caused by presence of different crystal lattice defects. The magnetic hyperfine and electron-deformation interactions are "orthogonal" to each other, and if a RE ion has a non-zero nuclear spin moment, the possibility to discover random strain effects in the optical spectra depends on a relation between the hyperfine splitting of a degenerate crystal-field level and the effective strain coupling constants proportional to the width of the strain distribution function. In particular, a specific doublet structure of a singlet-doublet transitions with a deep hole at the line center is observed in the optical absorption spectra of the impurity Tm^{3+} ions in $LiYF_4$,[8] however, it is not observed in the spectra of $CaWO_4$:Ho^{3+} (0.05 at.%) crystals with stronger random strains but with hyperfine splittings of the Γ_{34} doublets more than an order of magnitude larger than in Tm^{3+} ions. Nevertheless, the prominent effects due to random strains are observed in the EPR spectra of $CaWO_4$:Ho^{3+} (0.05 at.%) samples at the anticrossings with $\Delta m = 0$ and in the optical spectra of the samples containing higher concentrations of the impurity holmium ions.

Acknowledgements

The support by the Russian Foundation for Basic Research is acknowledged by EPC and MNP (grant No 13-02-01091) and by BZM (grant No 14-02-00826).

[a] Kazan E. K. Zavoisky Physical Technical Insitute, Kazan 420029, Russian Federation.
[b] Institute of Spectroscopy RAS, Troitsk 142190, Moscow, Russian Federation.
[c] Kazan Federal University, Kazan 420008, Russian Federation.
[d] St. Petersburg National Research University of Informational Technologies, Mechanics and Optics, St. Petersburg 197101, Russian Federation.

References

1 T. T. Basiev, *Physics of the Solid State,* 2005, **47**, 1354-1358.
2 S. Bertaina, S. Gambarelli, A. Tkachuk, I. N. Kurkin, B. Malkin, A. Stepanov and B. Barbara*, Nature Nanotechnology*, 2007, **2**, 39-42.
3 R. M. Rakhmatullin, I. N. Kurkin, G. V. Mamin, S. B. Orlinskii, M. R. Gafurov, E. I. Baibekov, B. Z. Malkin, S. Gambarelli, S. Bertaina and B. Barbara*, Phys. Rev. B: Condens. Matter Mater. Phys.*, 2009, **79**, 172408.
4 G. S. Shakurov, M. V. Vanyunin, B. Z. Malkin, B. Barbara, R. Yu. Abdulsabirov and S. L. Korableva, *Appl. Magn. Res.*, 2005, **28**, 251-265.
5 S. Bertaina, B. Barbara, R. Giraud, B. Z. Malkin, M. V. Vanyunin, A. I. Pominov, A. L. Stolov and A. M. Tkachuk, *Phys. Rev. B: Condens. Matter Mater. Phys.,* 2006, **74**, 184421.
6 D. E. Wortman and D. Sanders, *J. Chem. Phys.*, 1970, **53**, 1247-1257.
7 J. Kirton*, Phys. Rev.*, 1965, A **139**, A1930-A1933.
8 E. S. Grinberg, A. V. Dooglav and B. I. Kochelaev, *ZhETF*, 1982, **82**, 888-898 [*JETP*, 1982, **55**, 522-528]
9 S. A. Klimin, D. S. Pytalev, M. N. Popova, B. Z. Malkin, M. V. Vanyunin and S. L. Korableva*, Phys. Rev. B: Condens. Matter Mater. Phys.*, 2010, **81**, 045113.
10 D. S. Pytalev, E. P. Chukalina, M. N. Popova, G. S. Shakurov, B. Z. Malkin and S. L. Korableva, *Phys. Rev. B: Condens. Matter Mater. Phys.*, 2012, **86**, 115124.
11 B. Z. Malkin, D. S. Pytalev, M. N. Popova, E. I. Baibekov, M. L. Falin, K. I. Gerasimov and N. M. Khaidukov, *Phys. Rev. B: Condens. Matter Mater. Phys.*, 2012, **86**, 134110.
12 D. Errandonea and F. J. Manjón, *Progr. Mater. Science*, 2008, **53**, 711-773.
13 V. F. Tarasov and G. S. Shakurov*, Appl. Magn. Res.*, 1991, **2**, 571-576.
14 W. T. Carnall, G. L. Goodman, K. Rajnak and R. S. Rana, *J. Chem. Phys.*, 1989, **90**, 3443-3457.
15 C.-K. Loong, L. Soderholm, J. P. Hammonds, M. M. Abraham, L. A. Boatner and N. M. Edelstein, *J. Phys.: Condens. Matter*, 1993, **5**, 5121-5140.
16 V. V. Klekovkina, A. R. Zakirov, B. Z. Malkin and L. A. Kasatkina*, J. Phys.: Conf. Ser.*, 2011, **324**, 012036.

17 K. W. H. Stevens, *Proc. Phys. Soc., London, Sect.* A, 1952, **65**, 209-214.
18 B. Z. Malkin, Z. I. Ivanenko and I. B. Aizenberg, *Physics of the Solid State*, 1970, **12**, 1873-1880.
19 W.-C. Zheng, H.-N. Dong, X.-X. Wu and Sh. Tang, *Spectrochimica Acta,* 2004, A **60**, 3169-3171.
20 E. Bernal, *J. Chem. Phys*., 1971, **55**, 2538-2549.
21 D. E. Wortman and D. Sanders, *J. Chem. Phys*., 1970, **55**, 3212-3219.
22 B. Bleaney, P. M. Llewellyn, M. H. L. Pryce and G. R. Hall, *Phil. Mag*. , 1954, **45**, 991-992.
23 J. M. Baker and B. Bleaney, *Proc. R. Soc. Lond.*, 1958, A **245**, 156-174.
24 M. A. H. McCausland and I. S. Mackenzie, *Adv. Phys*., 1979. **28**, 305-456.
25 R. P. Gupta and S. K. Sen*, Phys. Rev. A*, 1973, **7**, 850-858.
26 A. Abragam and B. Bleaney, *Electron Paramagnetic Resonance of Transition Ions* (Oxford Univ. Press, Oxford, 1970).
27 M. N. Popova, E. P. Chukalina, B. Z. Malkin and S. K. Saikin, *Phys. Rev. B: Condens. Matter Mater. Phys.*, 2000, **61**, 7421-7427.
28 A. Baraldi, R. Capelletti, M. Mazzera, N. Magnani, I. Foldvari and E. Beregi, *Phys. Rev. B: Condens. Matter Mater. Phys.*, 2007, **76**, 165130.
29 M. Mazzera, R. Capelletti, A. Baraldi, E. Buffagni, N. Magnani and M. Bettinelli, *J. Phys.: Condens. Matter,* 2012, **24**, 205501.